Yi et al., http://www.jcb.org/cgi/content/full/jcb.201301004/DC1

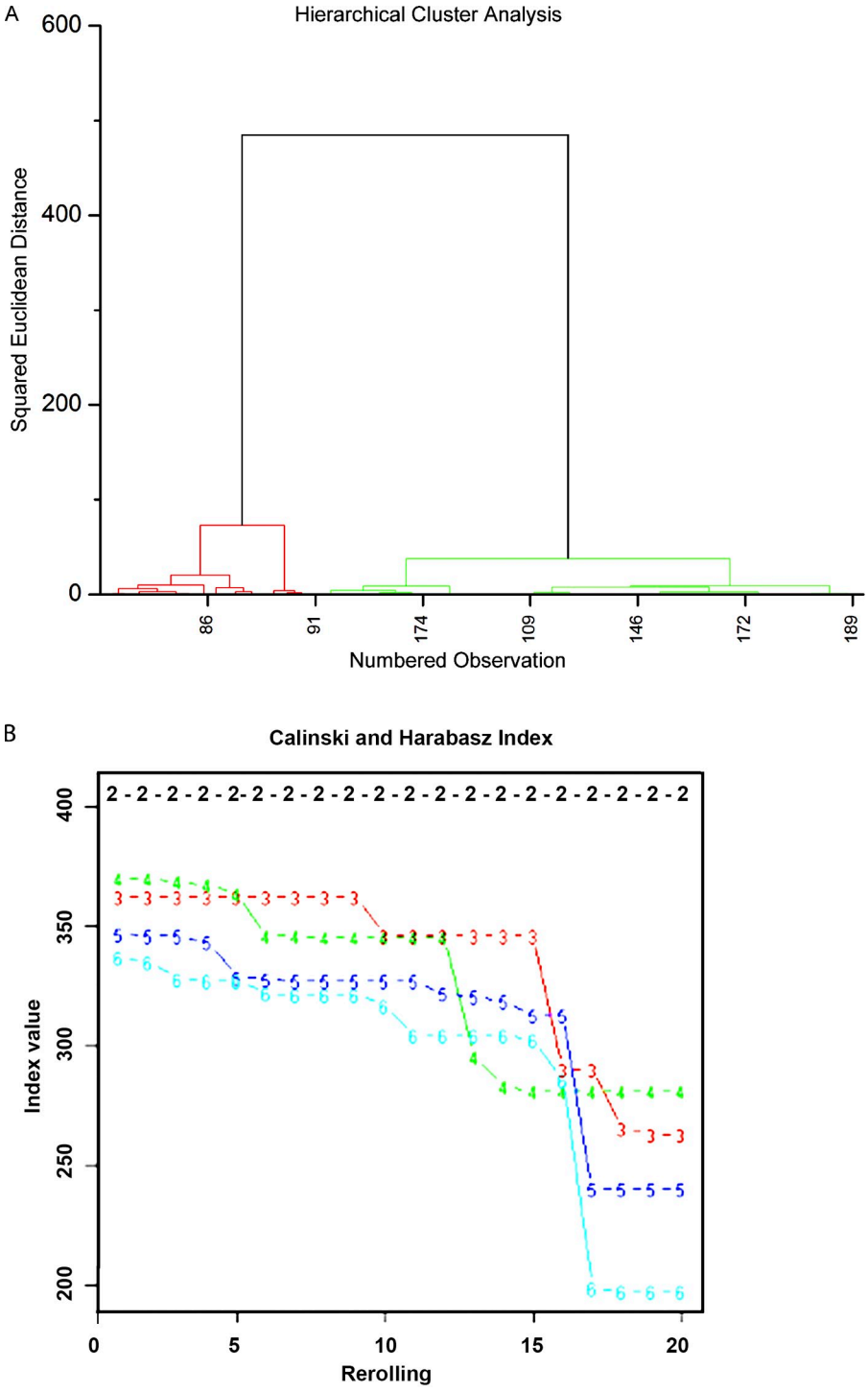

Figure S1. **Cluster analyses of the instantaneous MTOC speed data in Fig. 3 E argue that MTOC repositioning is biphasic.** (A) Shown is the dendrogram obtained from hierarchical cluster analysis of the instantaneous MTOC speed data in Fig. 3 E. The squared Euclidean distance on the y axis signifies the relatedness of each group of numbered observations. The largest change in squared Euclidean distance between successive levels of clustering provides the optimal number of clusters in the data sample. The two long black vertical lines in the dendrogram indicate that the kinetic data from Fig. 3 E fits best as two clusters. The green and red brackets under these two major branches contain the data points for the polarization and docking phases, respectively. (B) Shown is the Calinski and Harabatz Index chart, which is considered to be the most effective method for predicting the optimal number of clusters in a given dataset. The index value is shown on the y axis, and the rolling simulation number is shown on the x axis. The analysis was performed using the "fpc" package in R software, a Calinski and Harabatz Index of 2–6 cluster fits, and 20 rolling simulations. The figure shows that the two-cluster fit (indicated by the number "2" across the chart) scored the highest index value in all 20 simulations. Additional cluster analyses using the Silhouette Distance Index and the Davies and Bouldin Index also indicate that the kinetic data in Fig. 3 E separates optimally into two clusters (not depicted). Together, these statistical analyses argue that MTOC repositioning occurs in two distinct kinetic steps, i.e., that it is biphasic.

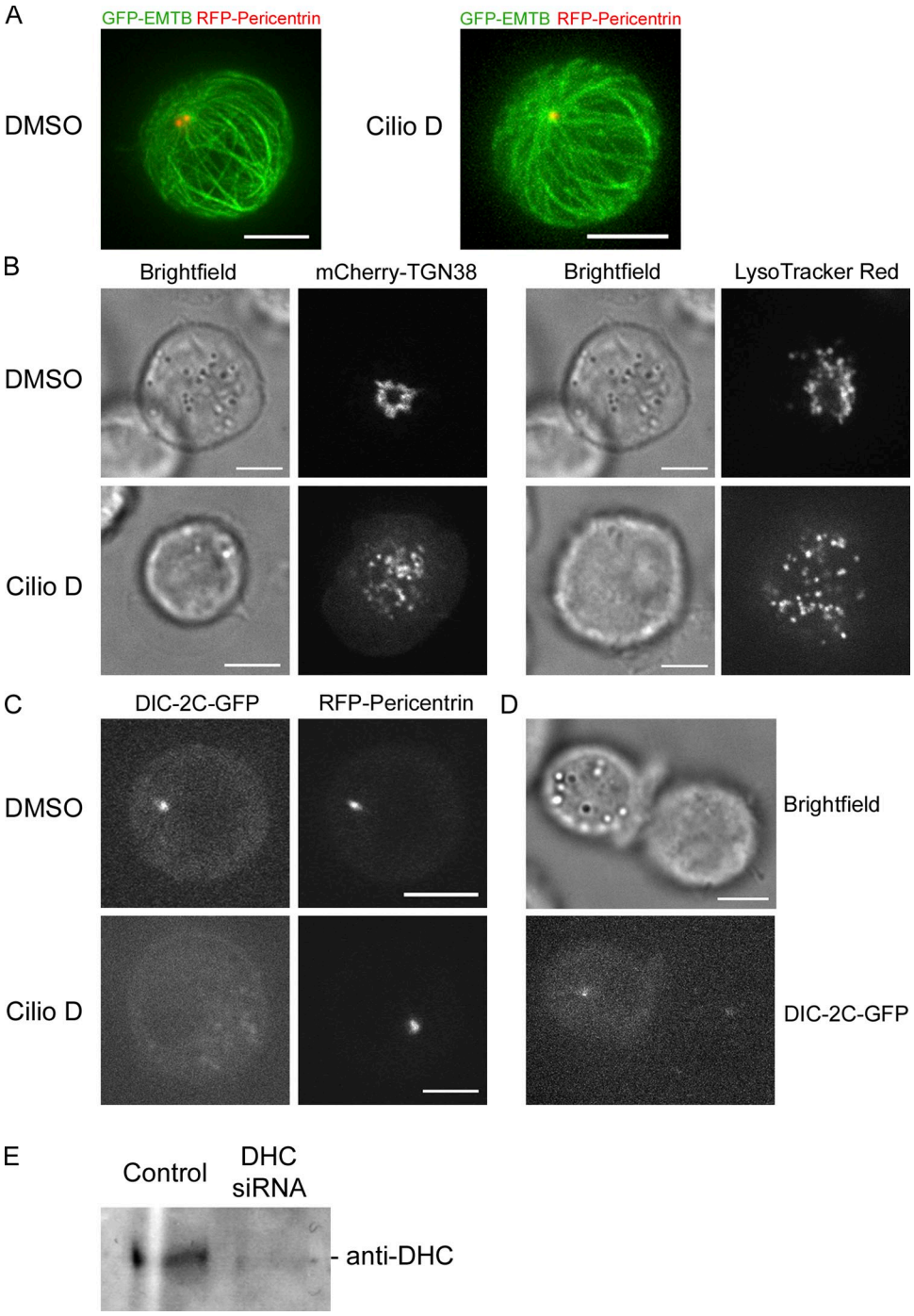

Figure S2. **Ciliobrevin-D treatment does not alter microtubule organization but does inhibit basic dynein functions and the accumulation of dynein at the centrosome.** (A) The overall organization of the microtubule cytoskeleton (imaged using GFP-EMTB), including the normal focusing of microtubule minus ends at the centrosome (imaged using RFP-Pericentrin), is preserved after 30 min treatment with 50 µM Ciliobrevin-D (compare the control DMSO-treated cell on the left to the Ciliobrevin-D–treated cell on the right). (B) 50 µM Ciliobrevin-D, but not DMSO (or the inactive Ciliobrevin analogue; not depicted), causes the dispersal of both the Golgi apparatus (left; imaged using mCherry-TGN38) and lysosomes (right; imaged using LysoTracker red) in Jurkat T cells. Both of these effects are associated with dynein inhibition in other cell types. Dispersal of the Golgi apparatus was observed in 65% of Ciliobrevin-D–treated cells (n = 66) compared with 14% of DMSO-treated cells (n = 28), whereas dispersal of lysosomes was observed in 83% of Ciliobrevin-D–treated cells (n = 42) compared with 9% of DMSO-treated cells (n = 45). (C) 50 µM Ciliobrevin-D, but not DMSO (or the inactive Ciliobrevin analogue; not depicted), causes a significant decrease in the normal accumulation of dynein (imaged using GFP-tagged dynein intermediate chain 2C [DIC-2C-GFP]) at the centrosome (imaged using RFP-Pericentrin). This was seen in 95% of treated cells (n = 20). Given that the steady-state accumulation of dynein at the centrosome is presumably due to its minus end–directed movement, this result is consistent with Ciliobrevin-D inhibiting dynein motility, as reported previously (Firestone et. al., 2012). (D) Localization of dynein imaged using DIC-2C-GFP in a T cell conjugated to a SEE+ Raji cell. Shown is a stack overlay of DIC-2C-GFP fluorescence throughout the entire volume of the T cell. Note that DIC-2C-GFP exhibits normal accumulation at the centrosome, but does not exhibit significant accumulation at the IS, in contrast to another study (Combs et. al., 2006). (E) Western blot of whole-cell extracts prepared from control and dynein heavy chain siRNA-treated Jurkats show ~90% reduction in dynein heavy chain protein level. The blot was probed with a dynein heavy chain antibody.

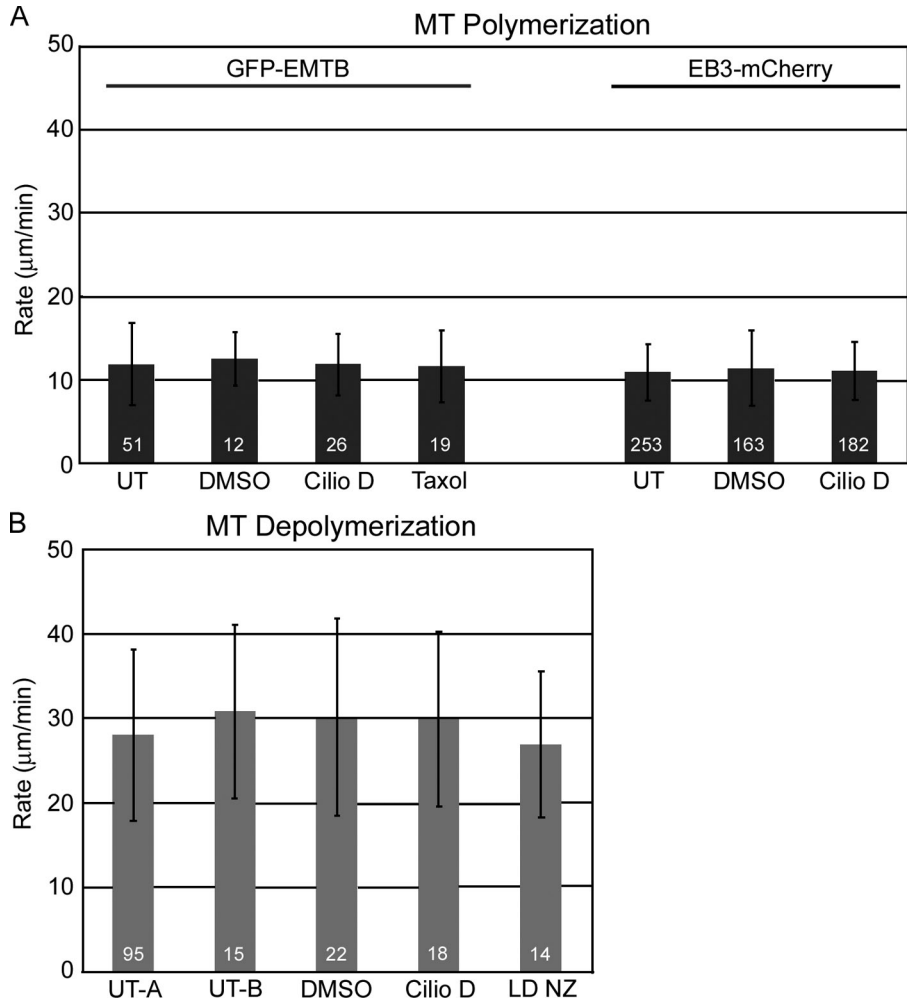

Figure S3. **Dynamics of the microtubule plus end in the presence of Ciliobrevin-D, taxol, or low dose nocodazole.** (A) Graph showing the rates of microtubule plus-end elongation in untreated (UT) cells and cells treated for 30 min with DMSO, 30 min with 50 µM Ciliobrevin-D, or 15 min with 0.5 µM taxol. The data for the four bars on the left were obtained using 3×GFP-EMTB to follow microtubule polymerization, whereas the data for the three bars on the right were obtained using EB3-mCherry to follow microtubule polymerization. (B) Graph showing the rates of microtubule plus-end depolymerization in untreated (UT-A and UT-B) cells and cells treated for 30 min with DMSO, 30 min with 50 µM Ciliobrevin-D, or 15 min with 100 nM nocodazole (LD NZ). The data for all of the bars except UT-B were obtained using GFP-EMTB to follow depolymerization, whereas the data for UT-B was obtained using mCherry-tubulin to follow depolymerization. The fact that the rate obtained using mCherry-tubulin (UT-B) is the same as the rate obtained using 3×GFP-EMTB (UT-A) argues that the expression of 3×GFP-EMTB does not stabilize microtubules. The numbers within each bar correspond to the number of microtubules measured.

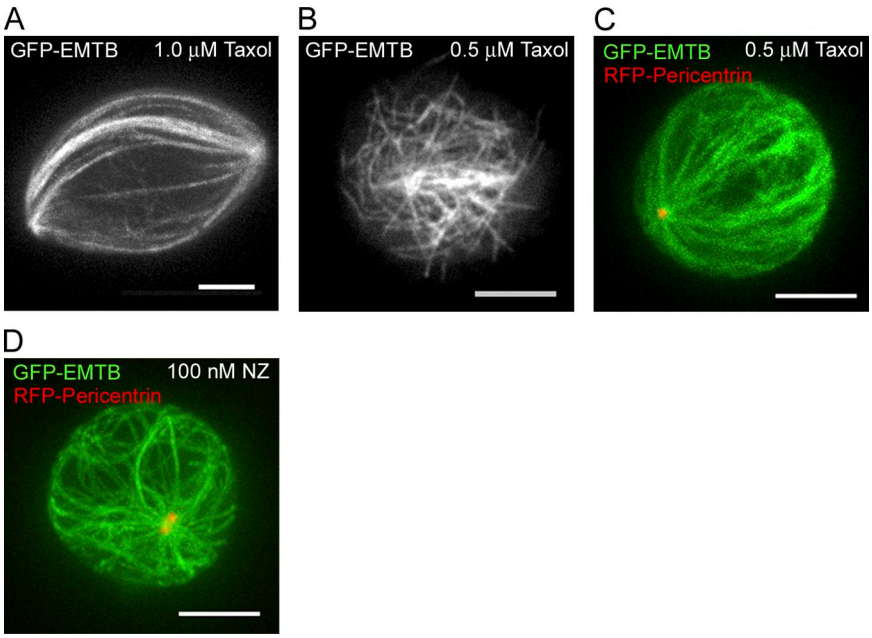

Figure S4. **0.5 µM taxol does not cause obvious microtubule bundling or defects in microtubule organization.** (A) Incubation of Jurkats in 1.0 µM taxol for 15 min leads to obvious microtubule bundling. (B) Microtubule bundling is not evident, however, in cells incubated for 15 min in 0.5 µM taxol (shown is a single focal plane near the bottom of a representative cell that was adhered to an anti-CD3–coated coverslip). Microtubules in these cells can grow, but exhibit little if any shortening/depolymerization (see Video 6; see also Fig. S3 and Table S1). (C) A stack overlay image across the entire cell volume of a representative Jurkat cell that was expressing RFP-Pericentrin to image the centrosome and 3×GFP-EMTB to image microtubules, and that had been treated for 15 min with 0.5 µM taxol, shows that this concentration of taxol does not disrupt microtubule organization, including the normal focusing of microtubule minus ends at the centrosome (this was seen in 100% of treated cells; $n = 50$). (D) A representative image of 3×GFP-EMTB fluorescence in a cell treated for 15 min with 100 nM NZ showing that while the dynamicity of microtubule ends has been lost (Table S1 B), the microtubule lattice is preserved.

Video 1. **Repositioning of the Jurkat T cell's centrosome toward the IS after contact with an APC that had been steered to the Jurkat using the optical trap.** The Jurkat cell was transfected with GFP-Cen-2 to mark the centrosome and the Raji B cell was coated with SEE. Images were acquired using a spinning disk confocal microscope (CSU-X1, Yokogawa Corporation of America; IX81, Olympus) and MetaMorph software, recorded at one frame every 15 s, and played back at 15 frames/s. Related to Fig. 1.

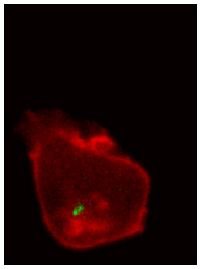

Video 2. **Repositioning of the Jurkat T cell's centrosome toward the IS after contact with an APC that had been steered to the Jurkat using the optical trap.** The Jurkat cell was transfected with GFP-Cen-2 and RFP-Farnesyl to mark the centrosome and IS membrane, respectively, and the Raji B cell was coated with SEE. Images were acquired using a spinning disk confocal microscope (CSU-X1, Yokogawa Corporation of America; IX81, Olympus) and MetaMorph software, recorded at one frame every 15 s, and played back at 15 frames/s. Related to Fig. 3.

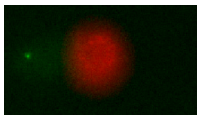

Video 3. **Protrusion of the APC's plasma membrane toward a stalled Jurkat T cell centrosome.** The Jurkat cell was transfected with GFP-Cen-2 to mark the centrosome, whereas the SEE-coated Raji B cell was labeled with PKH-26 to mark its plasma membrane. Images were acquired using a spinning disk confocal microscope (CSU-X1, Yokogawa Corporation of America; IX81, Olympus) and MetaMorph software, recorded at one frame every 15 s, and played back at 15 frames/s. Related to Fig. 4.

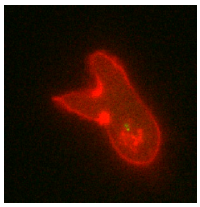

Video 4. **Invagination of the Jurkat T cell's plasma membrane toward its stalled centrosome.** The Jurkat cell was transfected with GFP-Cen-2 and RFP-Farnesyl to mark the centrosome and IS membrane, respectively, and the Raji B cell was coated with SEE. Images were acquired using a spinning disk confocal microscope (CSU-X1, Yokogawa Corporation of America; IX81, Olympus) and MetaMorph software, recorded at one frame every 15 s, and played back at 15 frames/s. Related to Fig. 4.

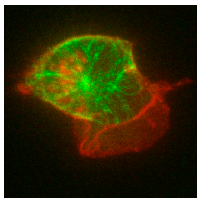

Video 5. **The dynamics of microtubules as the MTOC repositions toward the IS in a Jurkat T cell after contact with an APC that had been steered to the Jurkat using the optical trap.** The Jurkat cell was transfected with 3×GFP-EMTB and RFP-Farnesyl to mark microtubules and the IS membrane, respectively, and the Raji B cell was coated with SEE. Images were acquired using a spinning disk confocal microscope (CSU-X1, Yokogawa Corporation of America; IX81, Olympus) and MetaMorph software, recorded at one frame every 15 s, and played back at 15 frames/s. Related to Fig. 5.

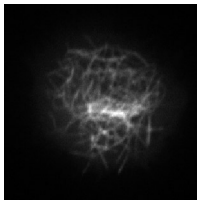

Video 6. **The dynamics of microtubules in a Jurkat T cell treated with 0.5 µM taxol and stimulated on an anti-CD3 antibody-coated coverslip surface.** The Jurkat cell was transfected with 3×GFP-EMTB to mark microtubules and stimulated in the presence of 0.5 µM taxol on a coverslip surface coated with OKT3 antibody. Images were acquired using a spinning disk confocal microscope (CSU-X1, Yokogawa Corporation of America; IX81, Olympus) and MetaMorph software, recorded at 1 frame every 4 s, and played back at 15 frames/s. Related to Fig. S4.

Table S1. **Inhibition of catastrophe events at the microtubule plus end by taxol and the dynamicity of microtubule plus ends by low dose nocodazole.**

A

Treatment	Catastrophe	N
Untreated	81%	42
DMSO	88%	52
Taxol	1%	103
Ciliobrevin-D	95%	40
Low Dose NZ	80%	25

B

Treatment	EB3 Comets/min	N
Untreated	45.4 ± 12.7	12
DMSO	50.3 ± 14.0	12
Ciliobrevin-D	41.9 ± 13.3	12
Low Dose NZ	0.5 ± 0.9	14

(A) Shown are the percentages of total microtubule plus ends observed during a two-minute time period that underwent catastrophe in Jurkat T cells expressing GFP-EMTB and adhered to an anti-CD3 antibody–coated coverslip. End dynamics were recorded using a spinning disc confocal microscope and a z0.5 µm optical section positioned just above the glass. Data were obtained for untreated cells and cells treated for 30 min with DMSO, 15 min with 0.5 µM taxol, 30 min with 50 µM Ciliobrevin-D, or 15 min with 100 nM nocodazole (Low Dose NZ). N values correspond to the total number of microtubule plus ends viewed. Note the dramatic decrease in catastrophe frequency in cells treated with taxol. The frequency of catastrophes in Ciliobrevin-D– and Low Dose NZ–treated cells was, on the other hand, very similar to that seen in untreated cells. We note that we could not measure rates of catastrophe or rescue using the standard method (inverse of the mean time spent in elongation/shortening before catastrophe/rescue) due to the high density of microtubules near the IS, and to the fact that most dynamic microtubules enter or exit the focal plane quickly because Jurkats are primarily round. This is in contrast to the situation at the periphery of flat tissue culture cells, which are typically used to measure microtubule dynamics. (B) Shown is the number of EB3-GFP comets that appeared during a one-minute time period in a single confocal section at the bottom of cells (N values correspond to the total number of cells viewed). Data were obtained for untreated cells and cells treated for 30 min with DMSO, 30 min with 50 µM Ciliobrevin-D, or 15 min with 100 nM nocodazole (Low Dose NZ; see also Fig. S3).

References

Combs, J., S.J. Kim, S. Tan, L.A. Ligon, E.L. Holzbaur, J. Kuhn, and M. Poenie. 2006. Recruitment of dynein to the Jurkat immunological synapse. *Proc. Natl. Acad. Sci. USA*. 103:14883–14888. http://dx.doi.org/10.1073/pnas.0600914103

Firestone, A.J., J.S. Weinger, M. Maldonado, K. Barlan, L.D. Langston, M. O'Donnell, V.I. Gelfand, T.M. Kapoor, and J.K. Chen. 2012. Small-molecule inhibitors of the AAA+ ATPase motor cytoplasmic dynein. *Nature*. 484:125–129. http://dx.doi.org/10.1038/nature10936